American Mineralogist, Volume 78, pages 699–709, 1993

Structure of silicate melts at high temperature: In-situ measurements in the system BaO-SiO_2 to 1669 °C

BJORN O. MYSEN
Center for High Pressure Research, Geophysical Laboratory, 5251 Broad Branch Rd. NW, Washington, DC 20015-1305, U.S.A.
JOHN D. FRANTZ
Geophysical Laboratory, 5251 Broad Branch Rd. NW, Washington, DC 20015-1305, U.S.A.

ABSTRACT

The structure of glasses, melts, and supercooled melts in the system BaO-SiO_2 with $BaO/SiO_2 = 0.367$ has been investigated in-situ with Raman spectroscopy from 25 to 1669 °C. For this purpose a technique has been developed that integrates confocal micro-Raman spectroscopy with a microheating stage that fits on the sample stage of a petrographic microscope. The temperatures are precise to ±4 °C and accurate to 5–10 °C. The excited volume is ~1 μm in diameter by 20–50 μm in depth.

The Raman spectra of room-temperature glasses and of melts and supercooled melts at higher temperatures are consistent with the presence of SiO_3^{2-} (or Q^2), $Si_2O_5^{2-}$ (or Q^3), and SiO_2 (or Q^4) units coexisting in the samples at all temperatures. No evidence for changes in types of structural units was found. The Raman spectra indicate that the abundance at SiO_3^{2-} and SiO_2 units increases, whereas that of $Si_2O_5^{2-}$ decreases with temperature. Under the assumption of ideal mixing, the high-temperature data are fitted in terms of ln K vs. $1/T$ (K), which yields a ΔH for the reaction $Si_2O_5^{2-} \leftrightarrow SiO_3^{2-} + SiO_2$ of 34 ± 4 kJ/mol.

INTRODUCTION

Description of the structure of magmatic liquids at high temperature is necessary for characterization of melt properties needed to understand magma formation and evolution. For example, viscous behavior (and related transport properties, e.g., diffusion and conductivity) of silicate melts can be described accurately with the configurational entropy model (Richet, 1984; Richet and Neuville, 1992). Although the model can be used to describe observed viscous behavior, prediction of melt viscosity based on the model requires accurate information on the abundance of structural units in the melts and how the unit distribution affects the configurational entropy at the temperature of interest.

Activity coefficients for chemical components such as, for example, SiO_2, can be derived from liquidus phase relations in specific systems. It has been shown that simple compositional variations, such as alkali or alkaline earth, have significant effects on the activity coefficients of these components (e.g., Ryerson, 1985). Without translation of this information into the thermodynamic behavior of the individual structural units at the liquidus temperature of interest, it is difficult to extend this information into realistic modeling of liquidus phase relations. Furthermore, quantitative, high-temperature melt structure data are required in modeling of liquidus phase relations and element partitioning between melts and minerals in magmatic systems. Models based on ad-hoc assumptions of melt structure have been proposed (e.g., Nielsen et al., 1988), but their reliability depends on the validity of the structural assumptions and without independent determination of melt structure may lead to erroneous conclusions (Ellison and Hess, 1989; see also Nielsen and Gallahan, 1990; Ellison and Hess, 1990).

The melt structure data bases currently available are severely limited, however, in part because of the technical difficulties associated with the high-temperature (magmatic temperature) spectroscopy needed to obtain the relevant structural data. For certain forms of spectroscopy (e.g., NMR), relaxation times are on the order of the time scale of the resonance at magmatic temperatures ($\sim 10^{-1}$ s) and thus render the techniques impractical as a structural probe for in-situ structure determination at most temperatures relevant to magmatic processes. Nevertheless, a few data have been reported (Stebbins, 1988; Farnan and Stebbins, 1990). Raman spectroscopy does not suffer from this limitation because the time scale of Raman scattering is on the order of 10^{-13} s, but until recently high-temperature Raman spectroscopy of silicate melts was impractical because of severe problems of sample degradation during extended exposure to high temperature and signal obliteration due to black-body radiation from the sample and furnace. Despite such problems, a few high-temperature data have been reported (Seifert et al., 1981; Takahashi et al., 1992; McMillan et al., 1992).

In order to obtain the large data base needed for structural characterization of magmatic liquids, a structural probe that overcomes these practical problems is needed. In this report, we describe a micro-Raman microheater system that, coupled with new, greatly enhanced signal

0003–004X/93/0708–0699$02.00

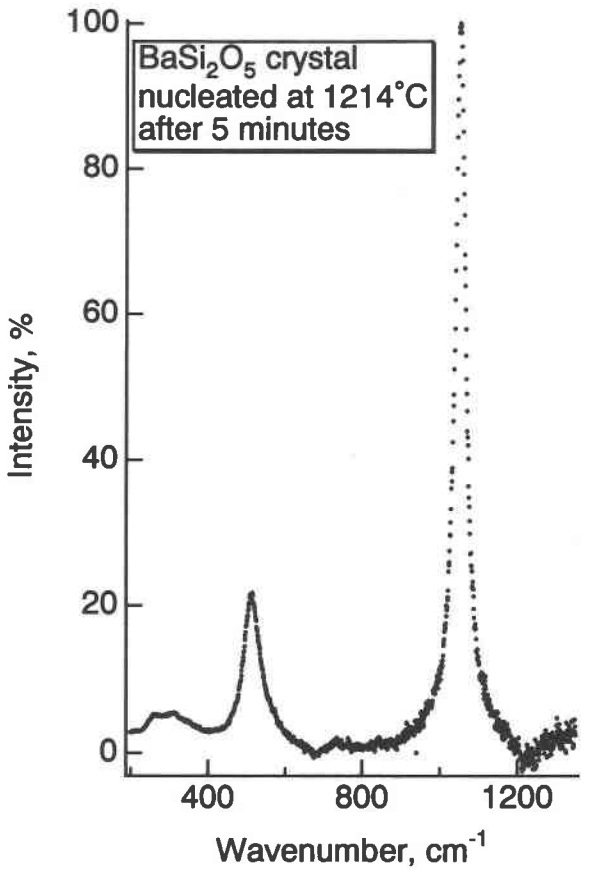

Fig. 1. Unpolarized Raman spectrum of partially crystalline sample at 1214 °C after 5 min at this temperature.

detection devices, has greatly reduced or perhaps eliminated the problems previously associated with Raman spectroscopy at high temperature. With this system, spectra can be obtained routinely and quickly ($\leq$1 min per spectrum) to temperatures exceeding 1700 °C at 1 bar. The capabilities will be illustrated with melt structural data for a composition in the system BaO-SiO_2 (Greig, 1927), whose liquidus temperature is near 1400 °C and has a glass transition temperature near 850 °C.

Experimental technique

Most of the compositions in previous high-temperature studies of melt structure were chosen primarily by their relatively low liquidus temperatures (e.g., alkali silicates), which reduced the technological barriers associated with the high-temperature spectroscopy. The principal problems were (1) sample degradation resulting from exposure of large sample surfaces (relative to volume) to high temperature over extended time periods (often several hours per spectrum), (2) heat shielding of optical and electronic components from high-temperature furnace environments, and (3) in certain forms of spectroscopy (e.g., Raman) the presence of black-body radiation from comparatively large furnaces and samples.

These problems were overcome by integrating a microheating stage with the focusing capability of a confocal micro-Raman system equipped with multichannel rather than single-channel detection systems. The heart of the system is a miniaturized heater (resembling a typical heating stage attached to a petrographic microscope) that takes advantage of two essential features of the confocal micro-Raman system. These are (1) the focus and positioning of the laser beam ($\leq$1 μm diameter on the sample), and (2) the confocal optical system itself, with which the depth of focus even in a clear sample such as silicate melts can be reduced to a few tens of micrometers.

The glass and melt samples and the positioning of the laser in the sample were monitored optically through the microscope before, during, and after all experiments. By monitoring the sample during an experiment, crystallization of glasses and supercooled liquids will be immediately evident. Onset of crystallization is also evident in the spectra themselves (Fig. 1). The spectrum in Figure 1 was taken 5 min after a melt was cooled rapidly ($\sim$100 °C/s) from 1500 to 1214 °C ($\sim$200 °C below the liquidus and $\sim$250 °C above the glass transition temperature). The narrow Lorentzian lines typical for spectra of crystalline materials are evident. Most likely the crystal is $BaSi_2O_5$, as this is the liquidus phase for the melt composition used in the present experiments (see further discussion of starting compositions below).

The confocal micro-Raman system plays a central role in rejecting stray light (e.g., black-body radiation) from sources other than the melt volume in the optical focus. Black-body radiation from a transparent material such as a silicate melt is comparatively small even at temperatures above 1600–1700 °C. Radiation does emanate, however, from bubble and melt surfaces, and also from the furnace itself. The positioning of the laser beam in the focal plane is done by optical imaging of the beam on the focal plane as observed through the microscope. The confocal system provides a means by which to reduce the focal depth in the sample. In this system, the laser point source is imaged on (or in the case of a melt, within) the sample. The Raman scattered light is directed to an adjustable pinhole (confocal hole in Fig. 2) located in the image plane of the microscope. The pinhole, which filters the laser beam, and the one used to transmit the Raman signal are the confocal diaphragms. These are optically conjugated with the sample in the image plane of the microscope so that only light from the focal plane (sample) reaches the detection system. In this fashion, the confocal system discriminates between light from the sample in focus and light from sources in deeper or shallower segments of the melt. With the objective lens (50×, 0.55 N.A.) used in our experiments, the diameter of the laser beam is approximately 1 μm. The depth of focus depends on the diameter of the adjustable confocal hole (adjustable from 0 to 1800 μm diameter; Fig. 2) and is in the range of 20–50 μm in the present experiments. Thus, black-body radiation from sources other than this volume $\sim$1 μm in diameter by 20–50 μm deep will not be transmitted to the detector.

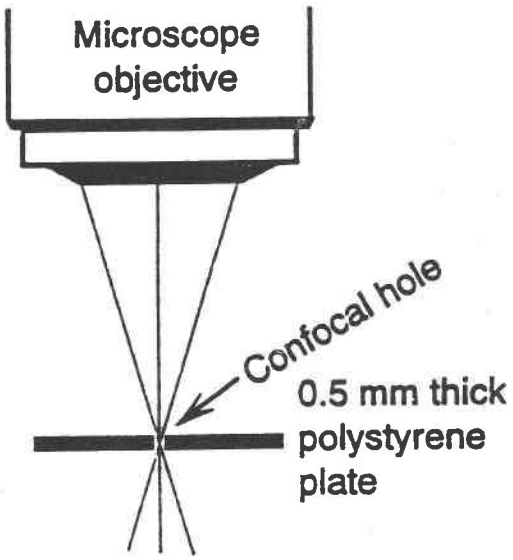

Fig. 2. Schematic illustration of confocal system.

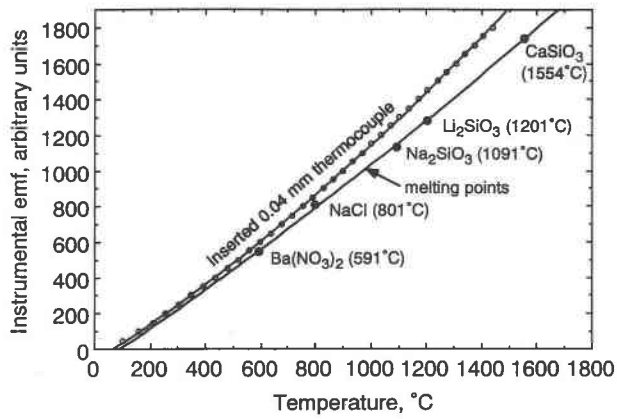

Fig. 3. Calibration data for microheater. The compounds used for calibration based on melting points (with melting temperature shown) are marked.

The heater-thermocouple is fabricated from two pieces of 0.8-mm Pt and $Pt_{90}Rh_{10}$ wire, which are welded and flattened to a thickness of 500 μm at the join. The Pt-$Pt_{90}Rh_{10}$ heater-thermocouple serves a dual function as both a thermocouple and heater (Ohashi and Hadidiacos, 1976). Heating takes place during the first half of every 60-Hz power-line cycle, and an emf is measured during the second half. The heater responds to applied power in a matter of seconds. A hole 1 mm in diameter is drilled through the junction. After a sample is melted into the hole, it is held in place by surface tension during high-temperature experiments.

Although the emf from the thermocouple yields an approximate temperature (principal uncertainties are introduced by electrical connections between dissimilar metals and alloys in the signal path between the hot spot of the furnace itself and the control unit), accurate temperature calibration is achieved by calibration of the emf against melting points of known compounds (Fig. 3). Initially a Pt-$Pt_{90}Rh_{10}$ thermocouple 0.04 mm in diameter was inserted into the melt for temperature measurement (Mysen and Frantz, 1992). This thermocouple acts, however, as a heat sink and so its recorded temperature is lower than that of the sample. This effect becomes more pronounced the higher the temperature (Fig. 3). More accurate calibration based on melting points was conducted with the samples exposed to the laser beam both with and without power settings between 100 and 850 mW at the sample. No discernible effect of laser power on the melting temperatures could be observed. The temperatures measured with this design are precise to within 4 °C anywhere within the sample over a time period of hours. The temperature accuracy, as determined by monitoring a melt-crystal interface passing through the sample from the furnace-sample boundary to the middle of the furnace hole as power is applied, is 5–10 °C.

The microheater is placed on the microscope stage of a custom-designed microscope port of a Dilor XY confocal micro-Raman system equipped with an EG&G Model 1433-C cryogenic charge coupled detector (CCD) and an intensified diode array detector (IPDA). For the high-temperature experiments reported here, the CCD provided a superior peak to background ratio (between 10/1 and 50/1) and was used for most of the measurements. The samples were excited with the 488- and 514-nm lines of a SpectraPhysics model 2025 Ar^+ ion laser operating near 850 mW at the sample. With this system, quality spectra were recorded in 10–60 s with the CCD within a single detector window. (The width of a detector window is governed by grating density, spectral range, wavelength of the excitation line, and the number of pixels in the detector. In the present experiment, the window width translated to 500–600 cm^{-1}. Whenever a wider spectral range was needed, individual windows are connected numerically. The IPDA detector was used when this need arose because unions of individual windows from the CCD are less precise than those from the IPDA detector.) Acquisition times with the IPDA detector were 3–5 min.

A melt composition (denoted BSU with 48 wt% BaO and 52 wt% SiO_2) in the system BaO-SiO_2 near the barium disilicate + tridymite eutectic (eutectic temperature, ~1370 °C; see Greig, 1927) was chosen to test the limitations of the system. From spectroscopic studies of glasses (Mysen et al., 1982a), the coexisting structural units in this composition (the bulk NBO/Si of the glass is 0.734) are of Q^2, Q^3, and Q^4 type. The nonbridging O per Si, nbo/si, of these individual units is 2, 1, and 0, respectively (nonbridging O per Si of individual structural units are indicated with lower case, nbo/si, whereas the nonbridging O per Si in the bulk melts and glasses is indicated by upper case, NBO/Si). Thus, the material consists of the same structural units as those commonly present in silicate melts compositionally relevant to natural magmatic liquids (Mysen, 1988).

Spectra of glasses were taken before and after the series of high-temperature measurements to determine whether

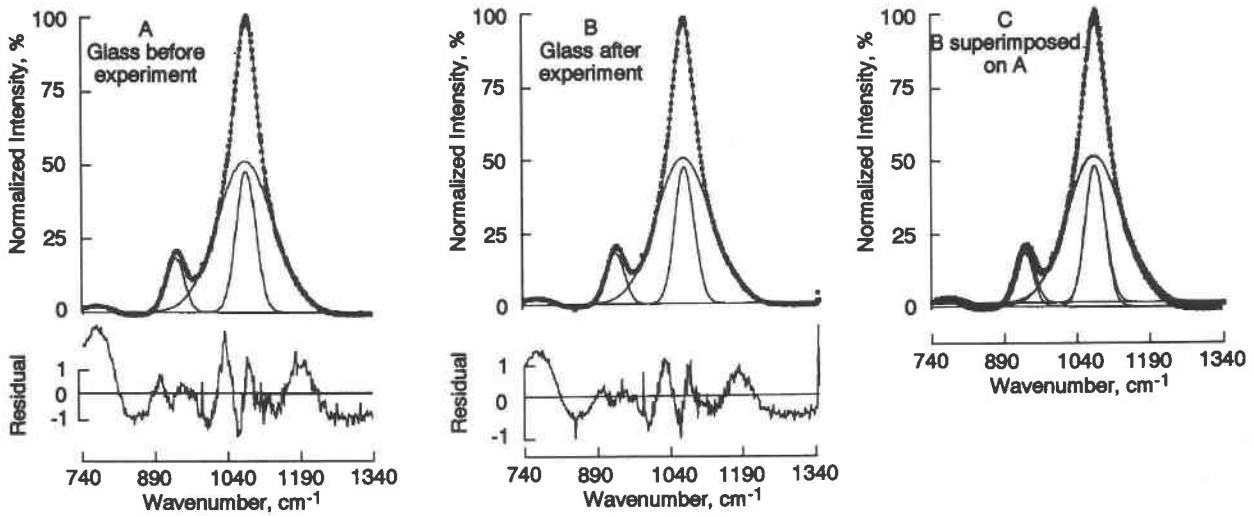

Fig. 4. Unpolarized Raman spectra of BSU composition glass before (**A**) and after (**B**) high-temperature experiments. In diagram **C** the spectra and fitted curves of **A** and **B** are superimposed.

the samples degraded (composition changed) during an experiment. If the melt composition changed during heating, this change is reflected in changes in the spectra of the quenched samples recorded after the high-temperature measurements. The curve-fitted spectrum (see also below for further discussion of curve-fitting procedures) of starting glass is compared with that taken after quenching to room temperature from the highest temperature (1669 °C) used in this study after acquisition of all the Raman spectra (Fig. 4). Both the data themselves and the lines fitted to the spectra of the two glasses are identical, thus leading to the conclusion that the composition of the sample used here was not altered by exposure to the high temperatures used in this study.

The samples were monitored optically through the microscope before, during, and after an experiment to ensure that visually evident sample changes (e.g., bubble formation and crystallization) did not occur. It was found, for example, that in the temperature range 800–1250 °C ($T_g \sim 850$ °C for this composition) nucleation and growth commenced within about 60 s after the sample was brought from above the liquidus to the desired temperature. Quality spectra in this temperature range could not be obtained with the IPDA detector, but the CCD was sufficiently fast that spectra could be taken before nucleation occurred. The procedure was as follows. Before each measurement, the sample was brought to melting at 1550 °C, followed by lowering the temperature to the desired value at ~100 °C/s. Spectral acquisition times were 10–20 s. The sample was monitored microscopically for crystallization (780× magnification), and the Raman spectrum was inspected for evidence of crystalline materials (e.g., Fig. 1).

Structural information was obtained from statistical analysis of Raman spectra of the melts. The spectra were corrected for temperature- and frequency-dependent scattering intensity (e.g., Long, 1977) prior to statistical analysis. Instrumental background was subtracted from spectra before temperature correction by least-squares fitting of a line through the data points at frequencies at which no Raman scattering was observed. The intensities were then normalized to the data point of the greatest absolute intensity. The curve fitting itself (Seifert et al., 1982; Mysen et al., 1982b) was carried out with the method of minimization of least squares with the algorithm written by Davidon (1966).

In the curve fitting all line parameters (frequency, half-width, and intensity) and the number of lines fitted to a spectrum are independent and unconstrained variables in the fitting routine. The number of lines fitted to a spectrum is treated statistically by numerical minimization of the squares of the deviations between the observed and the calculated Raman envelopes and by maximizing the randomness of the residuals. The principal three considerations were as follows. (1) The number of lines was determined by evaluating the effect of varying their number on the value of χ^2. The appropriate number of lines was defined as that where additional lines did not improve χ^2 significantly. A significant decrease in χ^2 is an approximately 10% decrease per additional line (Hamilton, 1965). Fewer than four lines results in rapid deterioration of the residual distribution and a rapid increase in the value of χ^2 (Fig. 5A–5C). Additional lines did not improve the goodness of fit. Also shown in Figure 5A–5C is the influence of the number of fitted lines of the calculated abundance of individual structural units (assignments and calculation procedures are described below). (2) The line shape was evaluated by monitoring the influence of a Lorentzian component on the goodness of fit (Fig. 5D). On the basis of these tests, it was decided to use pure Gaussian lines, as is common for Raman spectra of amorphous materials (e.g., Seifert et al., 1981;

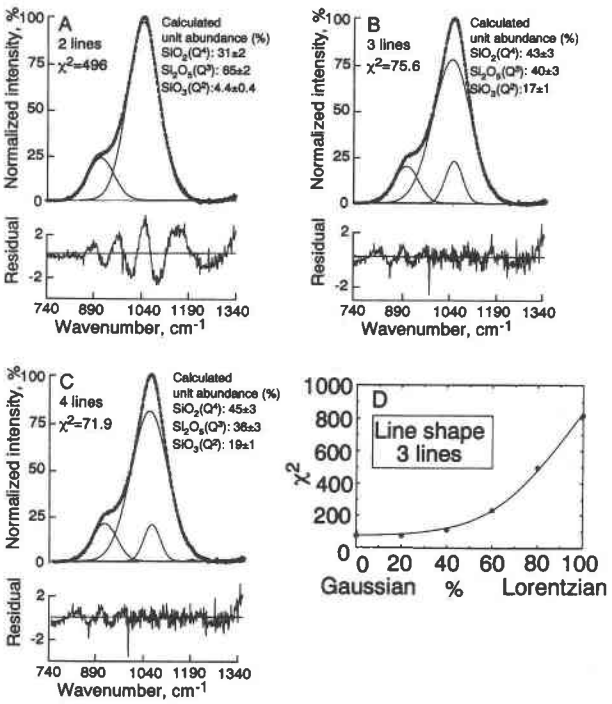

Fig. 5. Examples of two-, three-, and four-line fits to high-frequency envelope of unpolarized Raman spectrum of BSU melt taken at 1535 °C (**A–D**). (**D**) Effect of percent Lorentzian component on the χ^2 of the fit.

McMillan et al., 1982, 1992; Mysen et al., 1982a, 1982b; McKeown et al., 1984; Domine and Piriou, 1986; Lines et al., 1987). (3) As to whether the converged fits represent global or regional minima, that was evaluated by varying the values of the input parameters (trial values) randomly in the curve-fitting routine.

Results

Temperature-corrected spectra are shown in Figures 6 and 7. The spectra in Figure 6 cover the entire range of first-order Raman scattering in these glasses and melts. Those spectra were taken at temperatures above (>1250 °C) and below (<800 °C) those where nucleation was not a problem over the 3–5 min required to record the spectra (IPDA was used as a detector). Figure 7 shows the high-frequency region of the spectra (recorded with the CCD) from room temperature to 1669 °C, including those where nucleation occurred when the samples remained at temperature typically for periods longer than 60 s (see also detailed discussion of these problems in the section on experimental methods). In accord with previous observations (e.g., Seifert et al., 1981; Mysen and Frantz, 1992; McMillan et al., 1992), the overall topological features of the spectra of silicate melts and glasses do not differ greatly with a sharp band centered near 1100 cm^{-1} and a less intense band near 950 cm^{-1}. At lower frequency (see Fig. 6), the relative intensities of the two peaks between ~500 and 600 cm^{-1} change with increasing temperature. The higher frequency peak (near 600 cm^{-1}) exhibits increasing intensity with increasing temperature. Similar features were observed by McMillan et al. (1992) in spectra of KS2 ($K_2O \cdot 2SiO_2$) and KS4 ($K_2O \cdot 4SiO_2$) composition. They advanced a suggestion that the intensity increase near 600 cm^{-1} might reflect increased abundance of siloxane rings with increasing temperature, but other interpretations (Si-O-Si bending in depolymerized structural units) of this frequency region are also possible (e.g., Lazarev, 1972; Furukawa et al., 1981; Mysen et al., 1982a; Hemley et al., 1986). Regardless of the interpretation chosen, it is important to note that, at least on the basis of a visual inspection of the spectra recorded at different temperatures, there is no evidence for new bands in this or the high-frequency region (800–1300 cm^{-1}). Thus, it is unlikely that new structural units in the melts formed as the temperature was increased and the glass transformed from a glass to a melt.

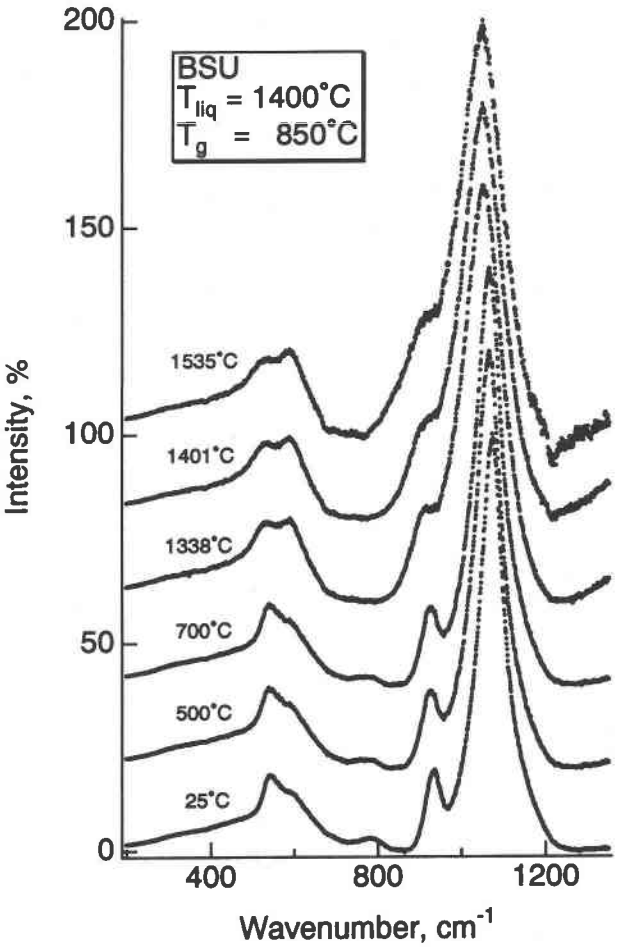

Fig. 6. Unpolarized Raman spectra (corrected for background and temperature) of BSU glass, supercooled liquid, and melt at the temperature indicated on individual spectra. Each spectrum is normalized to 100% for the highest intensity data point within that spectrum. The individual spectra are offset vertically by 20% for visual clarity.

The high-frequency region of the spectra (~800–1300

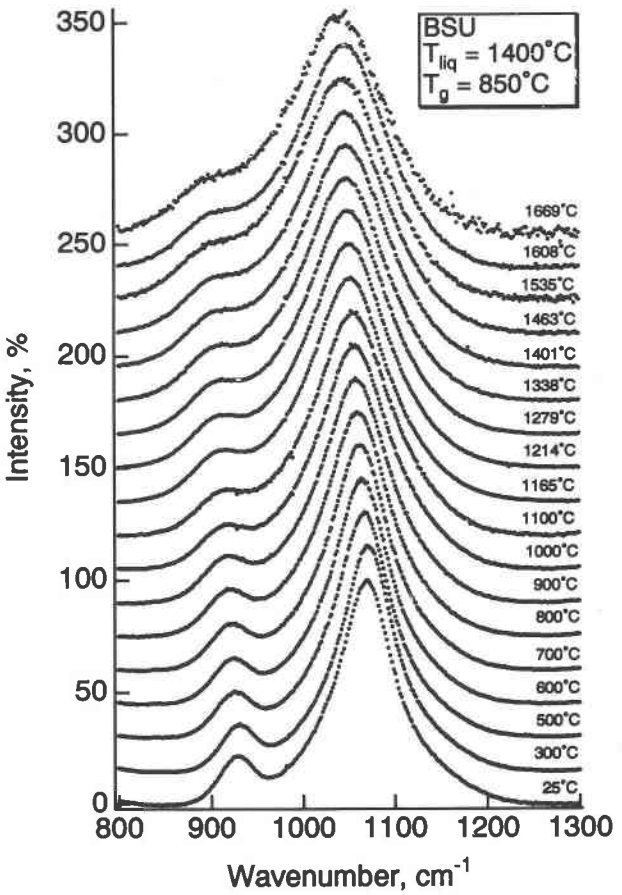

Fig. 7. Unpolarized Raman spectra (corrected for background and temperature) of composition BSU at the temperatures (°C) indicated. Each spectrum is normalized to 100% for the highest intensity data point within that spectrum. The individual spectra are offset vertically by 20% for visual clarity.

cm^{-1}) can be a sensitive indicator of the types and abundance of structural units (e.g., Brawer and White, 1975; Virgo et al., 1980; Mysen et al., 1982a; Mysen, 1990a, 1990b; McMillan et al., 1992). A qualitative description of most of the Raman spectra of the present samples in this spectral region as a function of temperature was provided by Mysen and Frantz (1992), and only a summary will be presented here. (Mysen and Frantz, 1992, discussed the spectrum of the glass at 25 °C and the spectra in the temperature range 1165–1669 °C. The spectra of samples from 300 to 1100 °C were recorded for the present study. It should be noted that because Mysen and Frantz, 1992, used an inserted thermocouple to monitor the temperature, they reported temperatures that were too low. See the experimental methods section and Fig. 3 to evaluate this problem. The temperatures shown on the spectra in Fig. 7 have been corrected with the furnace calibration against melting points of known compounds.)

The spectra, whether of glasses or melts, generally show an asymmetry on the high-frequency side of the strong 1100-cm^{-1} band and a shoulder or less intense peak near 950 cm^{-1} (Fig. 6). An intensity increase of the 950-cm^{-1} peak with temperature is noted for all the samples (Fig. 7).

All the spectra were fitted to three Gaussian lines in the high-frequency region (see Fig. 8 for examples). The assignments of the Raman bands are based on a variety of Raman studies of alkaline earth and alkali silicate and aluminosilicate melt compositions. These assignments yield structural interpretations consistent with those from other spectroscopic techniques such as ^{27}Al and ^{29}Si NMR (see Mysen, 1988, 1990a, 1990b, for a summary of the relevant literature). The sharp band near 1100 cm^{-1} is assigned to Si-O^- stretching in units with nbo/t = 1, which are referred to as $Si_2O_5^{2-}$ and Q^3 units in the text (see also Brawer and White, 1975; Virgo et al., 1980; Furukawa et al., 1981; McMillan, 1984). The band near 950 cm^{-1} is assigned to Si-O^- stretching in units with nbo/t = 2 (see also Brawer and White, 1975; Furukawa et al., 1981), which are referred to as SiO_3^{2-} and Q^2 units in the text. In the lower-frequency region near 400–600 cm^{-1} (Fig. 4), there are two bands, the highest frequency of which (near 600 cm^{-1}) most likely is due to Si-O-Si bending vibrations in these structural units (e.g., Furukawa et al., 1981; Lazarev, 1972).

At temperatures above that of the glass transition (T_g), the integrated intensities of the bands at 950 and 1100 cm^{-1} are systematic functions of temperature. The 950-cm^{-1} band intensity increases, whereas that of the 1100-cm^{-1} band decreases (Fig. 9).

There is also a broad band near 1070 cm^{-1} whose intensity increases slightly with temperature (Figs. 8, 9). This band may be assigned to Si-O^0 from bridging O in the melts (Lasaga, 1982; Mysen, 1990a, 1990b), although Fukumi et al. (1990) and McMillan et al. (1992) suggested that this band may be assigned to an Si-O vibration in structural units associated with metal cations (alkali metals in their case). Whereas the bands at 950 and 1100 cm^{-1} are generally accepted as being caused by antisymmetric Si-O^- stretch vibrations in units with 2 and 1 NBO/Si, respectively, the cause of the bands at 1070 and 1150 cm^{-1} remains somewhat controversial (Matson et al., 1983; Mysen et al., 1982a; Fukumi et al., 1990; McMillan et al., 1992), as the only evidence suggesting that they are due to an Si-O^0 vibration is derived from the spectra of vitreous SiO_2 (Lasaga, 1982). A band occurs in this region, however, whether or not fully polymerized (Q^4) units occur in glasses. As a matter of fact, Mysen et al. (1982a) noted a band near 1070 cm^{-1} from compositions as polymerized as tectosilicate (as in vitreous SiO_2) to compositions as depolymerized as those with bulk melt NBO/Si = 3.95 (orthosilicate has NBO/Si = 4), where there is no evidence for fully polymerized units. This observation led them to suggest that this band could be assigned to an Si-O^0 stretch vibration in structural units that were not, by themselves, fully polymerized. It is clear, nevertheless, that this band assignment is problematic. Its presence is definitely required from the viewpoint of statistical deconvolution of symmetric Gaussian (or Lorentzian for that matter) lines, but the assignment is uncertain.

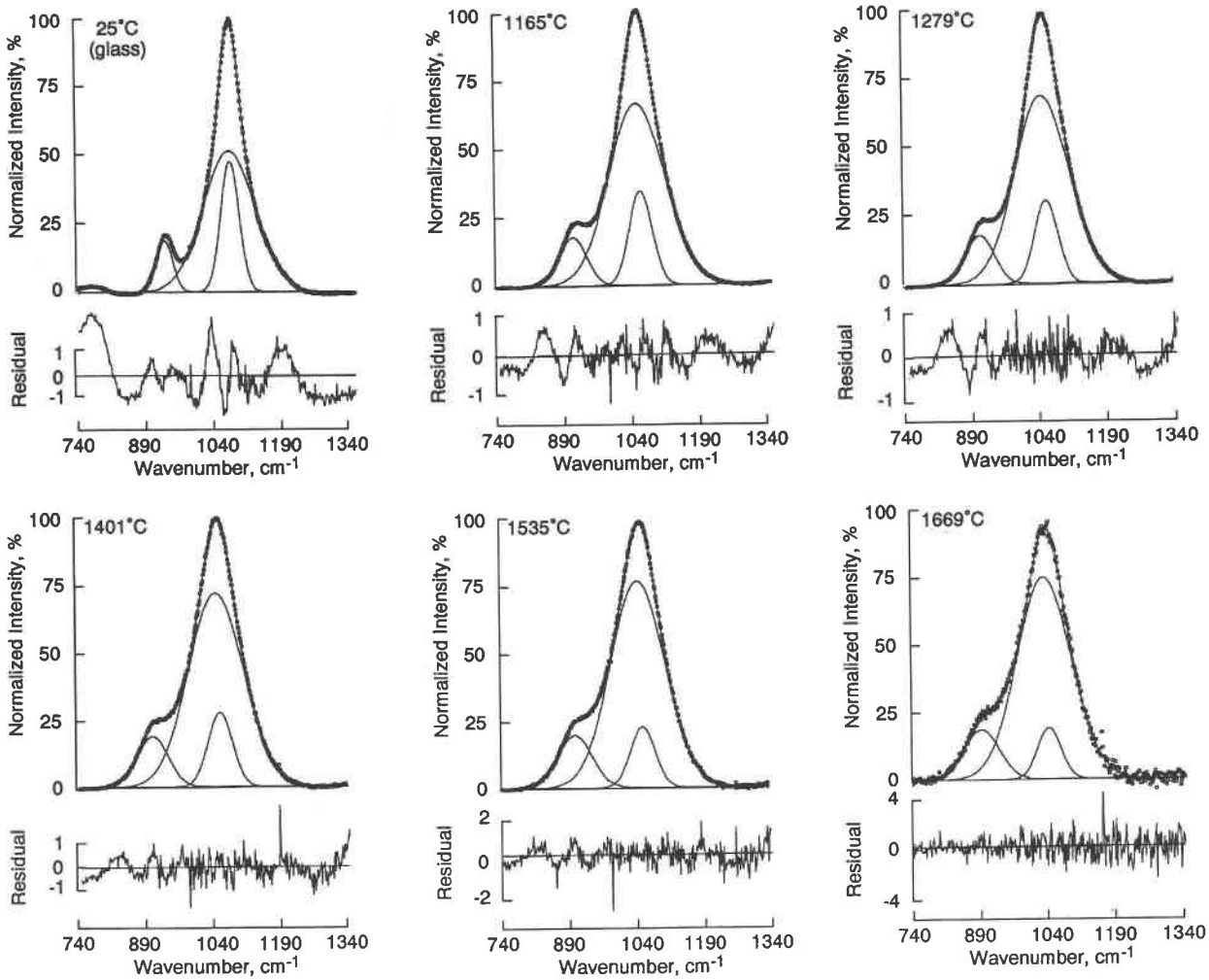

Fig. 8. Examples of curve-fitted spectra taken at the temperatures indicated.

All the nonbridging O in these melts and glasses resides in SiO_3 (Q^2) and Si_2O_5 (Q^3) structural units whose respective values of NBO/Si are 2 and 1. The overall NBO/Si of the melts and glasses is, however, 0.734. Therefore, there must also be at least one additional structural unit in these melts with NBO/Si < 0.734. Other vibrational and NMR spectroscopic data for alkali and alkaline earth silicate compositions in the same NBO/Si range indicate that this unit is of SiO_2 (or Q^4) type (e.g., Virgo et al., 1980; Mysen et al., 1982a; Stebbins, 1987; Matson et al., 1983). The band near 500 cm^{-1} in the low-frequency range (Fig. 4) could be assigned to S-O^0 rocking motions in such units (e.g., Bell and Dean, 1972; Revesz and Walrafen, 1983; Phillips, 1982, 1984). It has also been suggested that there would be a weak band between 1150 and 1200 cm^{-1} assigned to Si-O^0 stretching in such fully polymerized units (e.g., Mysen et al., 1982a), but inclusion of such a band in the curve fitting does not improve the quality of the fits significantly (e.g., Fig. 5). Coincidentally, Mysen et al. (1982a) suggested that the Raman cross section for this band is only about 10% of that of the bands at 1100 and 950 cm^{-1} bands. It is not surprising, therefore, that this band cannot be resolved in the present spectra.

Increasing temperature does not change the number of lines fitted to the high-frequency envelope of the spectra. Thus, it appears that major structural changes (e.g., different structural units) in the samples do not occur, as these are transformed from glass to supercooled melt and superliquidus melt. Therefore, a simple anionic equilibrium can be used to describe silicate melt and glass structure in the polymerization (NBO/Si) range between ~1.0 and near 0 (e.g., Virgo et al., 1980; Mysen et al., 1982a; Matson et al., 1983; Stebbins, 1987). The reaction

$$Si_2O_5^{2-}(2Q^3) \leftrightarrow SiO_3^{2-}(Q^2) + SiO_2\,(Q^4) \qquad (1)$$

adequately describes the anionic equilibrium among the structural units in these glasses and melts at least to the highest temperature of the present measurements (1669 °C).

Line frequencies (ν_i) and full width at half height (FWHH) generally are systematic functions of temperature (Fig. 10). The Raman frequencies are essentially linear functions of temperature (Fig. 10A) with $(1/\nu_i)(\partial\nu_i/\partial T)$

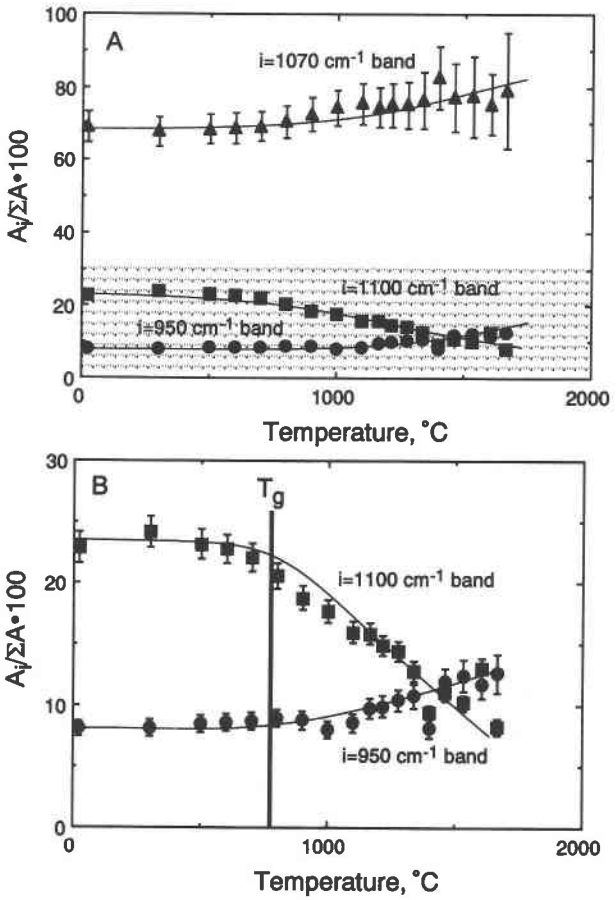

Fig. 9. (**A**) Area of the bands at 950, 1070, and 1150 cm^{-1} relative to the area of the entire high-frequency envelope (ΣA) as a function of temperature. (**B**) An expansion of the intensity relations among the 950 and 1100 cm^{-1} bands.

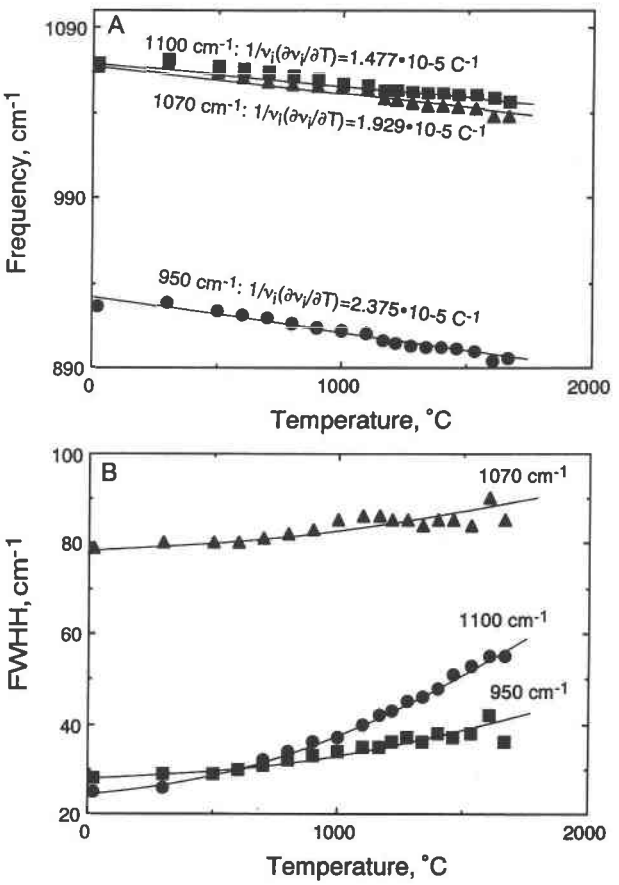

Fig. 10. Frequency (**A**) and full width at half height (FWHH) (**B**) of bands from structural units, indicated as a function of acquisition temperature.

between -1.4 and $-2.4 \cdot 10^{-5}$/°C. These values, resulting from the anharmonicity of the vibrational modes, compare well with those reported by McMillan et al. (1992) for KS2 and KS4 melts and glasses. The full width at half height (FWHH) for all but the bands increases systematically with temperature (Fig. 10B), presumably because of thermally induced broadening in distribution of bond angles (and bond lengths?).

Abundance of structural units

The abundance of the individual structural units in the melts as a function of temperature can be obtained from the Raman spectra. The simplest approach to this problem is to derive calibration factors for the integrated Raman intensities of appropriate bands by measuring spectra for which the abundance of the structural units has been obtained independently by, for example, ^{29}Si NMR or Raman spectroscopy, or both. With such an approach, Mysen (1990b) noted (see Fig. 4 in that paper) that Raman and NMR spectroscopy yield abundances that agree within the statistical error of the measurements. It should be noted, however, that because the quenching rate by which a glass is formed from a melt affects the fictive temperature, it is possible that the abundance of structural units in a glass used for calibration could depend on the quenching rate (e.g., Buckermann et al., 1992). In fact, Stebbins (1988), using ^{29}Si NMR spectroscopy to study the structural behavior of NS2 ($Na_2O \cdot 2SiO_2$) glass with fictive temperatures of 530 and 450 °C, reported a Q^4 abundance in these two glasses as 7.9 and 6.4 (± 0.5)%, respectively. The fictive temperature of 530 °C was from samples quenched at a reported rate of ~500 °C/s, whereas the glass at 450 °C was formed with a quenching rate on the order of 0.01 °C/s. The glass samples in the Na_2O-SiO_2 system used for calibration of Raman spectra for unit abundance determination (Mysen, 1990a, 1990b) were formed with quenching rates near 100 °C/s.

Calibration factors, θ_i, for integrated Raman intensities of appropriate Si-O^- stretch bands assigned to units, i, are developed as follows. (In these following expressions, Q notations are used to indicate the particular Raman band of interest. For the ~1100-cm^{-1} band, for example, the integrated area is denoted A_{Q^3}; for the ~950-cm^{-1} band, A_{Q^2}.) We first define calibration factors, θ_{Q^2} and

θ_{Q^3}, which are related to the mole fractions, X_{Q^2} and X_{Q^3}, and the areas of the bands at 950 and 1100 cm^{-1}, A_{Q^2} and A_{Q^3}, as follows:

$$\theta_{Q^3} = X_{Q^3}/A_{Q^3}, \quad \text{and} \quad \theta_{Q^2} = X_{Q^2}/A_{Q^2} \tag{2}$$

which yields the expression

$$\theta_{Q^3}/\theta_{Q^2} = (X_{Q^3}/X_{Q^2})(A_{Q^2}/A_{Q^3}). \tag{3}$$

The values of X_{Q^3}/X_{Q^2} and A_{Q^2}/A_{Q^3} needed to determine the $\theta_{Q^3}/\theta_{Q^2}$ ratio can be obtained from a standard where X_{Q^3}/X_{Q^2} is determined independently. An example of such a standard is $Na_2Si_2O_5$ (NS2) composition glass, where the combined ^{29}Si NMR and Raman data summarized by Mysen (1990a) yield $X_{Q^3}/X_{Q^2} = 13.4$ and $A_{Q^2}/A_{Q^3} = 0.218$. The calibration factor ratio then is

$$\theta_{Q^3}/\theta_{Q^2} = 2.92. \tag{4}$$

Equation 3 can be rearranged to express mole fractions of the structural units of an unknown:

$$(X_{Q^3}/X_{Q^2})^{unkn} = (\theta_{Q^3}/\theta_{Q^2})^{stand}(A_{Q^3}/A_{Q^2})^{unkn}. \tag{5}$$

In a composition such as BSU used here (with NBO/Si = 0.734), all nonbridging O atoms reside in Q^3 and Q^2 species. Therefore, the NBO/Si of the melt can be expressed as

$$(NBO/Si) = X_{Q^3}^{unkn} + 2X_{Q^2}^{unkn}. \tag{6}$$

From the $(\theta_{Q^3}/\theta_{Q^2})^{stand}$ calibrated with the NS2 glass standard and $(A_{Q^2}/A_{Q^3})^{unkn}$ obtained from the Raman spectra, the abundance of Q^2 and Q^3 species can be obtained by combining Equations 5 and 6. The abundance of fully polymerized structural units (Q^4 or SiO_2) can then be determined from the simple mass balance

$$X_{Q^4} = 1 - (X_{Q^3} + X_{Q^2}). \tag{7}$$

When applying these calibration factors to melts and glasses in the system BaO-SiO_2, it is assumed (1) that the calibration factors are insensitive to the different metal cation (Ba^{2+} in the unknowns as compared with Na^+ from the calibration samples) and (2) that these calibration factors are insensitive to the temperature at which the spectra were obtained. Mysen (1990a) found that even though in principle it would be expected that the type of metal cation should affect the Raman intensities, a comparison of calibrations derived from the spectra of glasses in the systems Na_2O-SiO_2 and K_2O-SiO_2 revealed no differences within the errors.

The second assumption, that the relative scattering intensity of the two Si-O^- stretch bands at 950 and 1100 cm^{-1} is independent of temperature in principle, is an approximation because the optic mode loss coefficient, α, is a function of temperature (e.g., Lines, 1987). The question is whether this dependence differs significantly for the two modes of interest. The function relating α to temperature is of the form

$$f(\alpha) = C \coth(h\omega/2kT) \tag{8}$$

where C is a constant for a specific mode (which includes a range of parameters specific to the mode in question), h and k are Planck's and Boltzmann's constants, ω is frequency, and T is temperature. If a temperature dependence of the relative Raman intensities used to calculate the abundance of structural units affects the data (outside the error in the intensity measurements), systematic changes of apparent unit distributions with temperature would be expected.

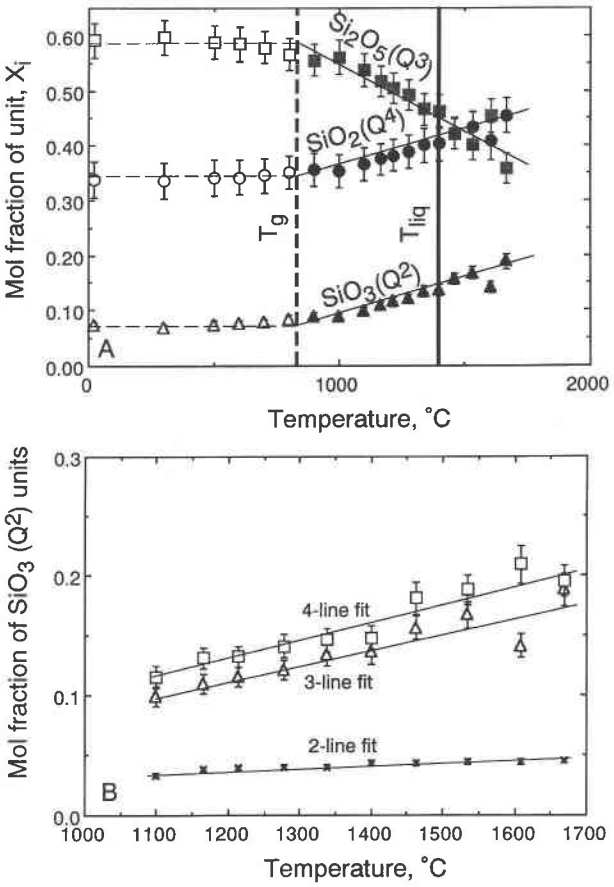

Fig. 11. (**A**) Abundance of structural units in the melts as a function of temperature as indicated. (**B**) Comparison of SiO_3 (or Q^2) abundance calculated from two-, three-, and four-line fits to the spectra (see Fig. 5), as marked on the figure.

The unit distribution as a function of temperature between 25 and 1669 °C is shown in Figure 11, where the approximate positions of the glass transition (T_g) and liquidus (T_{liq}) temperatures are also shown. These data (Fig. 11A) show that the abundance of the structural units is nearly independent of temperature from 25 °C to temperatures near that of the glass transition. This trend would not be expected if the relative intensities of the 950 and 1100 cm^{-1} varied with temperature. This absence of temperature-dependent unit distribution at temperatures below the glass transition is consistent, however, with the distribution of structural units being frozen in, at, or near T_g (Dingwell and Webb, 1990).

Above T_g it is evident that the abundance of the fully

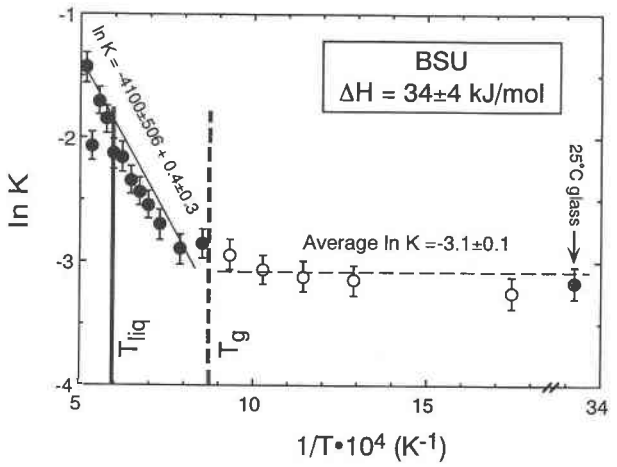

Fig. 12. The equilibrium constant for Reaction 1 as a function of temperature expressed as ln K vs. $1/T$ (K). The glass transition temperature is shown with a bar marked T_g and the liquidus temperature with a bar marked T_{liq}. Solid circles mark the data through which linear regression was conducted. The average ln K value for $T < T_g$ is from the temperatures less than that of the glass transition (including the room-temperature spectrum, 25 °C).

polymerized structural units (SiO_2 or Q^4) increases systematically with increasing temperature, whereas that of the structural units with NBO/Si = 1 ($Si_2O_5^{2-}$ or Q^3) decreases with increasing temperature. These changes are associated with a slight increase in the SiO_3^{2-} (Q^2) unit abundance. The evolution of the abundance with temperature is continuous across that of the liquidus (~1370 °C; see Greig, 1927).

Also shown in Figure 11 is a comparison of SiO_3 (or Q^2) abundance in BSU melts calculated from two-, three-, and four-line fits to the high-frequency envelope (see also Fig. 5). The general trend of increasing SiO_3 abundance with increasing temperature remains regardless of the number of lines chosen. The results from the three- and four-line fits are indistinguishable, whereas those from the statistically much poorer two-line fits (see Fig. 5) are lower. The general trend of increasing SiO_3 abundance with increasing temperature remains regardless of the number of lines chosen.

Under an assumption of ideal mixing of the structural units in the high-temperature melts, the equilibrium constant for Equation 1

$$K = X_{SiO_3^{2-}} \cdot X_{SiO_2} / X_{Si_2O_5^{2-}} \quad (9)$$

expressed as ln K vs. $1/T$ (Fig. 12), at temperatures above that of the glass transition follows the straight-line relationship expected from the simple expression

$$\ln K = -(\Delta H/RT - \Delta S/R). \quad (10)$$

The equilibrium constant, K, is insensitive to temperature within the uncertainty of the data from near that of the glass transition to room temperature. This observation differs slightly from that of McMillan et al. (1992) for KS2 and KS4 glasses. McMillan et al. (1992) suggested an apparent slight increase in calculated K values between T_g and room temperature and suggested that this increase may result from a small temperature dependence of the Raman cross sections for the bands at 950 and 1100 cm^{-1}. It was estimated that this temperature dependence would be equivalent to an ~2 kJ/mol overestimation of the ΔH values calculated for KS2 and KS4 melts. It should be noted, however, that McMillan et al. (1992) fitted only three Gaussian lines to the high-frequency envelope of their spectra (the 1050-cm^{-1} band was not included), thus possibly introducing a small error in the ln K vs. $1/T$ slope. Furthermore, McMillan et al. (1992) did not report uncertainties in the individual ln K vs. $1/T$ data points. Thus, it is not known whether their slight positive temperature for $T < T_g$ is within the error of the data. Within the error of the present data (Fig. 12) for BSU melt (its NBO/Si is ~0.75, which is intermediate, therefore, between that of KS2, with NBO/Si = 1, and KS4, with NBO/Si = 0.5), the temperature effect suggested by McMillan et al. (1992) cannot be discerned.

The ΔH derived from this relationship (Fig. 12) is 34 ± 4 kJ/mol. The ΔH for the barium silicate melt (with NBO/Si near 0.75) reported here compares with that of melt composition NA15 $\{(Na_2Si_2O_5)_{85} \cdot [Na_2(NaAl)_2O_5]_{15}$, by mol$\}$ with ~30 kJ/mol reported by Mysen (1990a). On the basis of the difference in species distribution determined by ^{29}Si NMR on slow-cooled ($5 \cdot 10^{-2}$ °C/s) and rapidly-cooled (~500 °C/s) NS2 glass, Brandriss and Stebbins (1988) suggested a ΔH value of 30 ± 15 kJ/mol for Reaction 1 for sodium disilicate melts. McMillan et al. (1992) reported 20.6 ± 5.5 kJ/mol for KS2 melt and supercooled liquid. It would appear, therefore, that the high-temperature, in-situ micro-Raman spectroscopic technique can be used routinely for quantitative description of the anionic structure of silicate melts.

Acknowledgments

Partial support for this research from the NSF-sponsored Center for High Pressure Research is acknowledged. Reviews by C.T. Prewitt and three anonymous reviewers are appreciated.

References cited

Bell, R.J., and Dean, P. (1972) Localization of phonons in vitreous silica and related glasses. In R.W. Douglass and B. Ellis, Eds., International conference on physics of non-crystalline solids, p. 443–452. Wylie-Intersciences, London.

Brandriss, M.E., and Stebbins, J.F. (1988) Effects of temperature on the structures of silicate liquids: ^{29}Si NMR results. Geochimica et Cosmochimica Acta, 52, 2659–2669.

Brawer, S.A., and White, W.B. (1975) Raman spectroscopic investigation of the structure of silicate glasses. I. The binary silicate glasses. Journal of Chemical Physics, 63, 2421–2432.

Buckermann, W.-A., Muller-Warmuth, W., and Frischat, G.H. (1992) A further ^{29}Si MAS NMR study on binary alkali silicate glasses. Glastechnische Berichte, 65, 18–21.

Davidon, W.C. (1966) Variable metric method for minimization (3rd edition), 21 p. Argonne National Laboratory ANL 5990, Lawrence Livermore.

Dingwell, D.B., and Webb, S.L. (1990) Relaxation in silicate melts. European Journal of Mineralogy, 2, 427–449.

Domine, F., and Piriou, B. (1986) Raman spectroscopic study of the SiO_2-Al_2O_3-K_2O vitreous system: Distribution of silicon and second neighbors. American Mineralogist, 71, 38–50.

Ellison, A.J.G., and Hess, P.C. (1989) Solution properties of rare earth elements in silicate melts: Inferences from immiscible liquids. Geochimica et Cosmochimica Acta, 53, 1965–1974.

——— (1990) Two-lattice models of trace element behavior: A response. Geochimica et Cosmochimica Acta, 54, 2297–2302.

Farnan, I., and Stebbins, J.F. (1990) A high temperature ^{29}Si investigation of solid and molten silicates. Journal of the American Ceramic Society, 112, 32–39.

Fukumi, K., Hayakawa, J., and Komiyama, T. (1990) Intensity of Raman band in silicate glasses. Journal of Non-Crystalline Solids, 119, 297–302.

Furukawa, T., Fox, K.E., and White, W.B. (1981) Raman spectroscopic investigation of the structure of silicate glasses. III. Raman intensities and structural units in sodium silicate glasses. Journal of Chemical Physics, 153, 3226–3237.

Greig, J.W. (1927) Immiscibility in silicate melts. American Journal of Science, 13, 1–44.

Hamilton, W.C. (1965) Significance of the crystallographic R-factor. Acta Crystallographica, 18, 502–510.

Hemley, R.J., Mao, H.K., Bell, P.M., and Mysen, B.O. (1986) Raman spectroscopy of SiO_2 glass at high pressure. Physics Review Letters, 57, 747–750.

Lasaga, A.C. (1982) Optimization of CNDO for molecular orbital calculation on silicates. Physics and Chemistry of Minerals, 8, 36–46.

Lazarev, A.N. (1972) Vibrational spectra and structure of silicates, 302 p. Consultants Bureau, New York.

Lines, M.E. (1987) Absolute Raman intensities in glasses. I. Theory. Journal of Non-Crystalline Solids, 89, 143–162.

Lines, M.E., Miller, A.E., Nassau, K., and Lyons, K.B. (1987) Absolute Raman intensities in glasses. II. Germania-based heavy metal oxides and global criteria. Journal of Non-Crystalline Solids, 89, 163–180.

Long, D.A. (1977) Raman spectroscopy, 276 p. McGraw-Hill, New York.

Matson, D.W., Sharma, S.K., and Philpotts, J.A. (1983) The structure of high-silica alkali-silicate glasses: A Raman spectroscopic investigation. Journal of Non-Crystalline Solids, 58, 323–352.

McKeown, D.A., Galeener, F.L., and Brown, G.E. (1984) Raman studies of Al-coordination in silica-rich sodium aluminosilicate glasses and some related minerals. Journal of Non-Crystalline Solids, 68, 361–378.

McMillan, P. (1984) Structural studies of silicate glasses and melts: Applications and limitations of Raman spectroscopy. American Mineralogist, 69, 622–644.

McMillan, P., Piriou, B., and Navrotsky, A. (1982) A Raman spectroscopic study of glasses along the joins silica-calcium aluminate, silica-sodium aluminate and silica-potassium aluminate. Geochimica et Cosmochimica Acta, 46, 2021–2037.

McMillan, P.F., Wolf, G.H., and Poe, B.T. (1992) Vibrational spectroscopy of silicate liquids and glasses. Chemical Geology, 96, 351–366.

Mysen, B.O. (1988) Structure and properties of silicate melts, 354 p. Elsevier, Amsterdam.

——— (1990a) Effect of pressure, temperature, and bulk composition on the structure and species distribution in depolymerized alkali aluminosilicate melts and quenched melts. Journal of Geophysical Research, 95, 15733–15744.

——— (1990b) Role of Al in depolymerized, peralkaline aluminosilicate melts in the systems Li_2O-Al_2O_3-SiO_2, Na_2O-Al_2O_3-SiO_2, and K_2O-Al_2O_3-SiO_2. American Mineralogist, 75, 120–134.

Mysen, B.O., and Frantz, J.D. (1992) Raman spectroscopy of silicate melts at magmatic temperatures: Na_2O-SiO_2, K_2O-SiO_2, and Li_2O-SiO_2 binary compositions in the temperature range 25°–1783°C. Chemical Geology, 96, 321–332.

Mysen, B.O., Virgo, D., and Seifert, F.A. (1982a) The structure of silicate melts: Implications for chemical and physical properties of natural magma. Reviews of Geophysics, 20, 353–383.

Mysen, B.O., Finger, L.W., Seifert, F.A., and Virgo, D. (1982b) Curve-fitting of Raman spectra of amorphous materials. American Mineralogist, 67, 686–696.

Nielsen, R.L., and Gallahan, W.E. (1990) In defense of the two-lattice model: A comment on Ellison and Hess. Geochimica et Cosmochimica Acta, 54, 2293–2295.

Nielsen, R.L., Davidson, P.M., and Grove, T.L. (1988) Pyroxene-melt equilibria: An updated model. Contributions to Mineralogy and Petrology, 100, 361–373.

Ohashi, Y., and Hadidiacos, C.G. (1976) A controllable thermocouple microheater for high-temperature microscopy. Carnegie Institution of Washington Annual Report, 75, 828–833.

Phillips, J.C. (1982) Spectroscopic and morphological structure of tetrahedral oxide glasses. Solid State Physics, 37, 93–171.

——— (1984) Microscopic origin of anomalously narrow Raman lines in network glasses. Journal of Non-Crystalline Solids, 63, 347–355.

Revesz, A.G., and Walrafen, G.E. (1983) Structural interpretation of some of the Raman lines from vitreous silica. Journal of Non-Crystalline Solids, 54, 323–355.

Richet, P. (1984) Viscosity and configurational entropy of silicate melts. Geochimica et Cosmochimica Acta, 48, 471–483.

Richet, P., and Neuville, D.R. (1992) Thermodynamics of silicate melts: Configurational properties. Advances in Physical Geochemistry, 10, 132–161.

Ryerson, F.J. (1985) Oxide solution mechanisms in silicate melts: Systematic variations in the activity coefficient of SiO_2. Geochimica et Cosmochimica Acta, 49, 637–651.

Seifert, F.A., Mysen, B.O., and Virgo, D. (1981) Structural similarity between glasses and melts relevant to petrological processes. Geochimica et Cosmochimica Acta, 45, 1879–1884.

——— (1982) Three-dimensional network structure in the systems SiO_2-$NaAlO_2$, SiO_2-$CaAl_2O_4$ and SiO_2-$MgAl_2O_4$. American Mineralogist, 67, 696–711.

Stebbins, J.F. (1987) Identification of multiple structural species in silicate glasses by ^{29}Si NMR. Nature, 330, 465–467.

——— (1988) Effects of temperature and composition on silicate glass structure and dynamics: Si-29 NMR results. Journal of Non-Crystalline Solids, 106, 359–369.

Takahashi, M., Toyuki, H., Tatsumisago, M., and Minami, T. (1992) High temperature Raman spectra of rapidly quenched $50Li_4SiO_4$, $50Li_2WO_4$ glass. Physics and Chemistry of Glasses, 33, 9–11.

Virgo, D., Mysen, B.O., and Kushiro, I. (1980) Anionic constitution of silicate melts quenched at 1 atm from Raman spectroscopy: Implications for the structure of igneous melts. Science, 208, 1371–1373.

Manuscript received March 5, 1992
Manuscript accepted March 19, 1993